Particle-hole configuration interaction and many-body perturbation theory: Application to Hg$^+$

J. C. Berengut

School of Physics, University of New South Wales, Sydney, New South Wales 2052, Australia

The combination of configuration interaction and many-body perturbation theory methods is extended to nonperturbatively include configurations with electron holes below the designated Fermi level, allowing us to treat systems where holes play an important role. For example, the method can treat valence-hole systems like Ir^{17+}, particle-hole excitations in noble gases, and difficult transitions such as the $6s \rightarrow 5d^{-1}6s^2$ optical clock transition in Hg$^+$. We take the latter system as our test case for the method and obtain very good accuracy ($\sim$1%) for the low-lying transition energies. The α dependence of these transitions is calculated and used to reinterpret the existing best laboratory limits on the time dependence of the fine-structure constant.

I. INTRODUCTION

The combination of configuration interaction and many-body perturbation theory (CI+MBPT) is a precise and flexible *ab initio* method to calculate atomic properties of few-valence-electron atoms and ions [1]. It treats the valence-valence electron correlations using CI, while core-valence correlations are treated using MBPT by adding corrections to the radial integrals in CI. However, several recent proposals have necessitated new methods of calculation in systems where holes play an important role and cannot be treated perturbatively. In this article we extend the CI+MBPT method to allow for arbitrary numbers of particles and holes while retaining the separation of correlation effects that allow us to apply MBPT.

The CI+MBPT method was first developed to treat neutral thallium as a three-valence-electron atom, which gave an accuracy well below 1% for the first few excitation energies [1]. Since then, it has been remarkably successful in treating a wide variety of two- and three-valence-electron atoms and ions and even some with four (e.g., [2–5]) and five valence electrons (Cr II [6]). Generally, as the number of valence electrons increases, the method becomes less effective, and one must revert to usual CI and estimate the core-valence correlations some other way (see, e.g., [7]). This is due to ever-increasing "subtraction diagrams": one wishes to use "spectroscopic" orbitals calculated in the V^N or V^{N-1} approximation, but the MBPT expansion then contains large one-body diagrams representing the difference between the Dirac-Fock potentials used to calculate the orbital and that of the closed-shell core. A V^{N-M} approximation was recommended in [8] in order to simplify the MBPT calculation for the core-valence correlations; however, then one must sacrifice the quality of the initial orbital, which can be problematic, particularly when treating open-shell systems.

The problem of large numbers of valence particles becomes even more acute when treating systems with nearly complete shells. It is here that the particle-hole CI+MBPT method presented in this paper can really help since in this case one may take the Fermi level as being above the open shell and treat the valence holes of the atom or ion using CI. Such systems with holes include Ir^{17+} [9], proposed as an optical clock [10], as well as less exotic species such as Ni II, which is seen in quasar absorption spectra [11]. Currently, these systems are treated as many-valence-electron systems using CI (e.g., [12]),

but the methods presented in this work should allow for more accurate treatment.

The particle-hole CI+MBPT can also be used for calculating metastable states of noble gases. Previous works have calculated low-lying spectra of noble gases using this type of formalism [13–16]; however, the treatment presented here is more flexible in that it allows for additional particle-hole excitations and valence "spectators".

This flexibility is a great strength of the particle-hole CI+MBPT method; we can take into account important excitations of electrons from below the Fermi level using either CI or MBPT, depending on how important the contribution of a shell is. As an example, consider the original CI+MBPT system, neutral thallium [1]. In that work to get good accuracy the $6s^2$ electrons had to be included in CI due to their strong interaction with the valence electron. In effect, Tl was treated as a three-valence-electron system, while MBPT was used to get core-valence correlations with shells below $6s^2$. The cost was the inclusion of subtraction diagrams since the valence orbitals were calculated in the V^{N-1} approximation while the V^{N-3} core was frozen at the CI level. With the current approach, we could keep the Fermi level above the $6s^2$ shell (i.e., using V^{N-1}) and still treat the excitations from the $6s^2$ shell nonperturbatively using particle-hole CI.

In this paper we test our method by calculating low-lying transitions in the Hg$^+$ ion, important because laser-cooled Hg$^+$ ions are used for both microwave [17] and optical [18] frequency standards. Calculations of energy levels, blackbody radiation shifts, and oscillator strengths were previously performed using both third-order relativistic many-body perturbation theory and the single-double all-order method [19], but crucially, the optical clock transition was not accessible using these methods. To lowest order the $6s \rightarrow 5d^{-1}6s^2$ clock transition can be described as a particle-hole excitation, with the valence $6s$ electron being a spectator. It is precisely this sort of system that our method is designed to treat.

One important use of the Hg$^+$ optical clock is to constrain potential drift in the value of the fine-structure constant, $\alpha = e^2/\hbar c$. Measurements of the frequency ratio of the ^{199}Hg$^+$ and Al$^+$ optical atomic clocks were taken several times over the course of a year [20]. The Hg$^+$ clock frequency is highly sensitive to the value of α, while the Al$^+$ is relatively insensitive. The resulting limit on $\dot{\alpha}/\alpha$ remains the tightest laboratory constraint on variations of fundamental constants,

but calculations of the α dependence of the Hg$^+$ transition are based only on configuration interaction calculations treating the ion as an 11-valence-electron system [21,22]. In this work we use the particle-hole CI+MBPT method to calculate the transition frequencies and α dependence of the low-lying transitions in Hg$^+$, including the clock transition. We use this to reinterpret the measurements of the Hg$^+$/Al$^+$ frequency ratio to obtain updated laboratory limits on $\dot\alpha/\alpha$.

This work is organized as follows. In Sec. II we introduce the particle-hole CI formalism and compare it against the usual "electron-only" CI for our Hg$^+$ test case. As expected, both methods give the same transition energies. We then add core-valence correlations using MBPT in Sec. III, which shows that only in the particle-hole formalism does the addition of MBPT improve the results for Hg$^+$. In Sec. IV we add some additional MBPT diagrams representing valence-valence correlations that arise in the particle-hole formalism. Finally, in Sec. V we calculate the α dependence of the Hg$^+$ transitions. Atomic units ($\hbar = m_e = |e| = 1$) are used throughout.

II. CONFIGURATION INTERACTION WITH HOLES

To start our calculation, we solve the self-consistent Dirac-Fock equations for the core electrons,

$$\hat{h}^{\rm DF}|m\rangle = \varepsilon_m|m\rangle, \tag{1}$$

where

$$\hat{h}^{\rm DF} = c\boldsymbol{\alpha}\cdot\boldsymbol{p} + (\beta - 1)c^2 - V^{N_{\rm core}}(r). \tag{2}$$

The potential $V^{N_{\rm core}}$ includes the nuclear potential (Z/r outside the nucleus and with finite-size corrections within it) and the electronic potential with both direct and exchange parts of the core electrons included in the self-consistent Hartree-Fock procedure. For the present Hartree-Fock calculation we include 78 core electrons in the configuration [Xe] $4f^{14}5d^{10}$. Here all shells are closed, but in general, we can sometimes obtain better starting orbitals by including a partially filled closed shell, as was done in previous works (e.g., [6,23]). However, we must then include MBPT subtraction diagrams (see Sec. III).

We then generate a single-particle basis set $|i\rangle$ by diagonalizing a set of B splines over $\hat{h}^{\rm DF}$ [24]. The resulting orbitals include core and valence orbitals and a large number of virtual orbitals (pseudostates), which we reduce in number by excluding those with the highest energy.

The many-electron basis is formed from configuration state functions (CSFs) denoted below with capital letters $|I\rangle$. Slater determinants are first formed from the orbitals $|i\rangle$. All Slater determinants with fixed angular momentum projection M corresponding to a configuration are diagonalized over the $\hat{J}^2$ operator, giving us CSFs with fixed angular momentum J and projection M.

The many-electron Hilbert space is separated into subspaces $\mathcal{P}$ and its complement $\mathcal{Q}$ ($\mathcal{P} + \mathcal{Q} = 1$). CSFs in the $\mathcal{P}$ space are included in the configuration interaction procedure directly, while those in the $\mathcal{Q}$ space are treated using many-body perturbation theory. In the CI method the many-electron wave function ψ is expressed as a linear combination of CSFs

from only the subspace $\mathcal{P}$:

$$\psi = \sum_{I\in\mathcal{P}} C_I|I\rangle. \tag{3}$$

The coefficients C_I are obtained from the matrix eigenvalue problem

$$\sum_{J\in\mathcal{P}} H_{IJ}C_J = EC_I, \tag{4}$$

where H_{IJ} is the matrix element of the exact Dirac-Coulomb Hamiltonian operator $\mathcal{H}$ projected onto the model subspace using the projection operator $\hat{\mathcal{P}}$:

$$\hat{\mathcal{P}}\mathcal{H}\hat{\mathcal{P}} = \sum_i c\boldsymbol{\alpha}\cdot\boldsymbol{p}_i + (\beta - 1)c^2 + e_i V^{N_{\rm core}}(r_i)$$
$$+ \sum_{i<j} \frac{e_i e_j}{|\boldsymbol{r}_i - \boldsymbol{r}_j|}. \tag{5}$$

Here i and j run over the valence electrons and holes, and e_i is -1 if i is an electron state (above the Fermi level) and $+1$ if it is a hole. The resulting energies E are therefore calculated with respect to the Fermi level; that is, the closed-shell core has $E = 0$.

We introduce a second quantization notation to separate $\mathcal{H}$ into one- and two-body operators (see [2] for details):

$$\mathcal{H}^{(1)} = \sum_{ij}\{a_i^\dagger a_j\}\langle i|\hat{h}^{\rm CI}|j\rangle, \tag{6}$$

$$\mathcal{H}^{(2)} = \frac{1}{2}\sum_{ijkl}\{a_i^\dagger a_j^\dagger a_l a_k\}\langle ij|r_{12}^{-1}|kl\rangle. \tag{7}$$

Here $a_i^\dagger$ and a_i are electron creation and annihilation operators, and the brackets $\{\cdots\}$ denote normal ordering with respect to the closed-shell core.

In previous works all CSFs in the valence space $\mathcal{P}$ had the same number of valence electrons. Our code, however, allows for additional particle-hole pairs, provided that the total fermion number is conserved. For example, our calculations of Hg$^+$ include CSFs based on configurations $|6s\rangle$, $|5d^{-1}6s^2\rangle$, and $|5d^{-2}6s\,6p^2\rangle$ (among many others). We express these using second quantization with respect to the Fermi level; the Wick contractions required to calculate matrix elements H_{IJ} were implemented in our atomic code AMBIT [23].

To test our code, we compare our particle-hole CI calculation for Hg$^+$ with a traditional CI calculation. To form the set of $\mathcal{P}$-space configurations used, we start with the leading configurations $|6s\rangle$, $|6p\rangle$, $|5d^{-1}6s^2\rangle$, $|5d^{-1}6p^2\rangle$, and $|5d^{-1}6s\,6p\rangle$. From these we take single-electron excitations up to $16spdf$ and allow an additional hole excitation in only the $5d$ shell. (The notation $16spdf$ refers to the highest principal quantum number for each wave, in this case $1 - 16s$, $2 - 16p$, etc. Note that higher orbitals are pseudostates.) We then allow a second electron excitation up to $10spdf$. For the traditional CI calculation, where the $5d^{10}$ shell is taken as valence above the Fermi level, this is equivalent to allowing single excitations from the leading configurations up to $16spdf$ and double excitations up to $10spdf$, but ensuring at least eight electrons remain in the $5d$ shell. The resulting CI matrices are rather large; for example, the $J = 5/2$ odd-parity matrix includes

TABLE I. Configuration interaction calculations of Hg$^+$ using traditional CI (electrons only) and the particle-hole CI. E is the valence binding energy, and Δ is the excitation energy relative to the $5d^{10}6s$ ground state. All energies are in cm^{-1}.

Level	J	Electrons only		Electrons and holes	
		E	Δ	E	Δ
$6s\ ^2S$	1/2	−9085835	0	−149653	0
$5d^{-1}6s^2\ ^2D$	5/2	−9047981	37854	−111840	37814
	3/2	−9032845	52990	−96704	52949
$6p\ ^2P^o$	1/2	−9036118	49717	−100187	49466
	3/2	−9027966	57869	−92112	57541
$5d^{-1}6s\,6p$	5/2	−9006616	79219	−70704	78949
$5d^{-1}6s\,6p$	7/2	−9001801	84034	−65907	83746
	5/2	−9001291	84544	−65396	84257
	3/2	−8999704	86131	−63846	85807

191 511 CSFs. However, the CI configuration set ($\mathcal{P}$ space) cannot be said to be saturated even in this case.

We present the comparison in Table I. The particle-hole method returns the single-electron binding energy of each low-lying level. The electron-only CI method returns the binding energy for 11 electrons (i.e., back to the Fermi level below $5d^{10}$). Both methods should give exactly the same level spacings; in fact, they are slightly different due to small numerical errors in the integration routines. Thus it is here that we see the first advantage of the particle-hole CI method: it is numerically stable because it does not rely on large cancellation of binding energies.

III. CI+MBPT

Our implementation of the CI+MBPT method [1] is described in detail elsewhere [2]. Omitting mathematical details, we write the exact Hamiltonian $\mathcal{H}$ in the subspace $\mathcal{P}$ using the Feshbach operator, which yields the exact energy when operating on the model function $\Psi_P = \hat{\mathcal{P}}\Psi$:

$$[\hat{\mathcal{P}}\mathcal{H}\hat{\mathcal{P}} + \Sigma(E)]\Psi_P = E\Psi_P. \qquad (8)$$

We can then generate a perturbation expansion for Σ in the residual Coulomb interaction, which to second order can be written in matrix form as

$$\Sigma_{IJ} = \sum_{M \in \mathcal{Q}} \frac{\langle I|H|M\rangle\langle M|H|J\rangle}{E - E_M}, \qquad (9)$$

where I and J enumerate CSFs from the model subspace $\mathcal{P}$. The final equation of the CI+MBPT method can be expressed as

$$\sum_{J \in \mathcal{P}} \left(H_{IJ} + \sum_{M \in \mathcal{Q}} \frac{\langle I|H|M\rangle\langle M|H|J\rangle}{E - E_M} \right) C_J = EC_I. \qquad (10)$$

Thus the method includes correlations with configurations in the $\mathcal{Q}$ space by changing the matrix elements in the $\mathcal{P}$-space CI calculation. In practice, we simplify this procedure by modifying the one- and two-particle radial integrals in Eqs. (6) and (7). A diagrammatic technique for calculating Σ is presented in [2] along with explicit expressions for the radial integrals.

In Table II we compare CI+MBPT calculations using the traditional CI method and the particle-hole method. In both CI calculations we consider orbitals below $5d^{10}$ as frozen (i.e., there are no configurations with holes in the $5s^2$, $5p^6$, $4d^{10}$, and $4f^{14}$ shells or those below them). Correlations with the frozen core are therefore treated using MBPT; excited orbitals up to $30spdfgh$ are included in the MBPT diagrams. $\Sigma^{(1)}$ calculations include MBPT modifications to the one-body integrals of (6); $\Sigma^{(1,2)}$ includes MBPT in both one-body and the two-body integrals (7), while $\Sigma^{(1,2,3)}$ also includes effective three-body core-valence integrals that occur in the second order of MBPT (see [23] for details).

Unlike in the pure CI calculations presented in Table I, there is no reason in this case that the two calculations should give the same result. Indeed, one of the purposes of this work is to avoid the large subtraction diagrams in $\Sigma^{(1)}$ that are partially canceled by terms in $\Sigma^{(2)}$ (see [6] for details). Subtraction diagrams are not present in the particle-hole calculation since in that case $\hat{h}^{\text{CI}} = \hat{h}^{\text{DF}}$ and there are no off-diagonal matrix elements of (6) (at least until MBPT corrections are included). Table II shows that the accuracy of the calculation of low-lying levels is improved by MBPT in the particle-hole calculation but not in the traditional electron-only calculation.
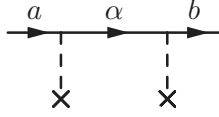
TABLE II. CI+MBPT calculations of excitation energies for Hg$^+$ using traditional CI (electrons only) and the particle-hole CI. Calculations including MBPT in one-body and two-body integrals are labeled $\Sigma^{(1)}$ and $\Sigma^{(1,2)}$, respectively, while $\Sigma^{(1,2,3)}$ includes effective three-body interactions. All energies are in cm^{-1}.

Level	J	CI	Electrons only			Electrons and holes			Expt.
			$\Sigma^{(1)}$	$\Sigma^{(1,2)}$	$\Sigma^{(1,2,3)}$	$\Sigma^{(1)}$	$\Sigma^{(1,2)}$	$\Sigma^{(1,2,3)}$	
$6s\ ^2S$	1/2	0	0	0	0	0	0	0	0
$5d^{-1}6s^2\ ^2D$	5/2	37814	17957	28432	32205	27197	34683	34721	35515
	3/2	52949	30698	44362	48001	41736	50095	50027	50556
$6p\ ^2P^o$	1/2	49466	49328	49356	51137	53494	52010	51908	51486
	3/2	57541	59358	55272	59952	62948	61297	61188	60608
$5d^{-1}6s\,6p$	5/2	78949	60024	69157	74890	71945	78727	78975	79705
$5d^{-1}6s\,6p$	7/2	83746	64567	74422	79825	77009	83164	83206	84212
	5/2	84257	65021	75326	80413	77442	83606	83727	84836
	3/2	85807	66882	76143	81850	79169	85142	85136	86178

FIG. 1. One-body valence-valence subtraction diagram $\Sigma_{\text{val}}^{(1)}$.

IV. MBPT CORRECTIONS TO VALENCE-VALENCE INTEGRALS

In previous implementations of CI+MBPT, the $\mathcal{Q}$ space is defined to include all configurations with holes in the core. Since the valence space does not include holes, this was a clear delineation. Now that we can include configurations with holes in the CI calculation, we must redefine the $\mathcal{Q}$ space. In this work we take the $\mathcal{Q}$ space to include any configurations with holes below the $5d^{10}$ shell (not including it) or with electron excitations above the valence space.

The particle-hole CI+MBPT method then allows for an additional type of diagram that has no additional core holes but does have electron excitations outside the valence space. At second order in the residual Coulomb interaction these valence-valence diagrams occur in the one-body, two-body, and effective three-body operators, as shown in Figs. 1–3. In these diagrams the external lines marked $a, b, \ldots$ are valence electrons or holes, while the internal lines marked α, β are virtual electron orbitals outside the CI valence space. Diagrams with external field lines [Figs. 1 and 2(b)] are known as subtraction diagrams since the one-body external field operator is $\hat{h}^{\text{CI}} - \hat{h}^{\text{DF}}$. In the current work these diagrams are zero since $\hat{h}^{\text{CI}} = \hat{h}^{\text{DF}}$. Note that hole-hole diagrams, where the virtual electron orbitals (α, β) are replaced with nonvalence holes, are included already; for example, Fig. 3(f) in [2] is Fig. 2(a) with α and β replaced with hole states.

Including valence-valence diagrams allows us to significantly reduce the size of the CI calculation. Table III shows the results of our smaller CI calculation in which, from the same set of leading configurations used in Secs. II and III, we allow double-electron excitations up to $10spdf$ and single-hole excitations in only $5d$ (as before). In this case the matrix size for the $J = 5/2$ odd-parity calculation is 57 879, much smaller than in the previous calculations which included additional single-electron excitations up to $16spdf$.

Table III shows that including valence-valence diagrams can bring smaller CI+MBPT calculations more in line with the larger ones, although clearly this can overshoot the experimental values. This may point to the possibility that a "converged" CI calculation using second-order MBPT with no
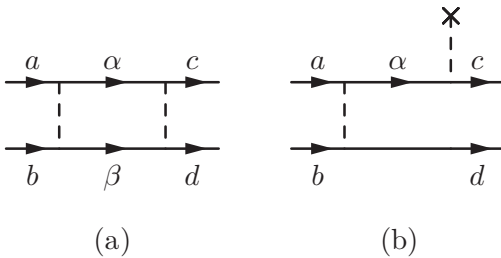

FIG. 2. Two-body valence-valence diagrams $\Sigma_{\text{val}}^{(2)}$. The subtraction diagram (b) represents four diagrams, with the complementary diagrams obtained by reflection in the horizontal and vertical planes.
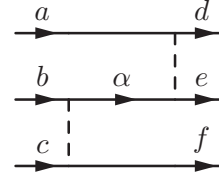

FIG. 3. Effective three-body valence-valence diagram $\Sigma_{\text{val}}^{(3)}$.

valence-valence diagrams might be similarly discrepant with the experiment. In any case the results strongly suggest that valence-valence diagrams can be of help in cases where the CI matrix grows very rapidly and it is not possible to even approach convergence.

V. DEPENDENCE ON THE FINE-STRUCTURE CONSTANT

We have calculated the dependence of the levels on the fine-structure constant α, usually expressed with the q value defined by

$$\omega(\alpha) = \omega_0 + qx, \tag{11}$$

where $x = (\alpha/\alpha_0)^2 - 1$ and ω_0 is the laboratory energy, with α given by its present-day value α_0. To calculate q we vary α directly in the code and extract the numerical derivative over x.

Our results are presented in Table IV. The value quoted for this work is the average of two methods: the large CI+$\Sigma^{(1,2,3)}$ from Sec. III and the CI+$\Sigma^{(1,2,3)}$+$\Sigma_{\text{val}}^{(2,3)}$ calculation of Sec. IV; both calculations give energies that are close to experiment and q values that are highly consistent. The error quoted is roughly half the difference between the two calculations: these should be taken as only indicative errors.

Of particular interest is the $6s\,^2S_{1/2}$–$5d^{-1}\,6s^2\,^2D_{5/2}$ transition at $\omega = 35\,515$ cm^{-1}, which is the reference transition for the NIST Hg$^+$ clock [18]. This transition was compared with the 37 93 cm^{-1} Al$^+$ clock [25,26] several times over the course of a year, and the frequency ratio $\nu_{\text{Al}^+}/\nu_{\text{Hg}^+}$ was found to vary by $(-5.3 \pm 7.9) \times 10^{-17}$/yr [20]. With the q value given in Table IV for the Hg$^+$ clock transition and taking the Al$^+$ q value from Ref. [27], we find that the sensitivity of the ratio to a fractional change in α is $-2.861\,(34)$.

TABLE III. Particle-hole CI+MBPT calculations of Hg$^+$ using a smaller basis for CI ($10spdf$) and $\Sigma^{(1,2,3)}$ (third column). The effect of adding Σ_{val} is shown in the fourth and fifth columns, which add $\Sigma_{\text{val}}^{(2)}$ [Fig. 2(a)] and $\Sigma_{\text{val}}^{(2,3)}$ [Figs. 2(a) and 3], respectively. All energies are in cm^{-1}.

Level	J	$\Sigma^{(1,2,3)}$	$+\Sigma_{\text{val}}^{(2)}$	$+\Sigma_{\text{val}}^{(2,3)}$	Expt.
$6s\,^2S$	1/2	0	0	0	0
$5d^{-1}\,6s^2\,^2D$	5/2	32418	31940	35121	35515
	3/2	47840	47201	50446	50556
$6p\,^2P^o$	1/2	53279	53654	53693	51486
	3/2	62671	63093	63188	60608
$5d^{-1}\,6s\,6p$	5/2	79221	80806	85917	79705
$5d^{-1}\,6s\,6p$	7/2	83211	83742	88486	84212
	5/2	83877	84534	89031	84836
	3/2	85018	85626	90558	86178

TABLE IV. Calculated dependence on the fine-structure constant q (cm^{-1}).

Level	J	E(cm^{-1}) Expt.	q (cm^{-1}) This work	Other
$6s\ ^2S$	1/2	0	0	
$5d^{-1}6s^2\ ^2D$	5/2	35515	$-50667(600)$	-56670[a]
				-52200[b]
	3/2	50556	$-35960(600)$	-44000[a]
				-37700[b]
$6p\ ^2P^o$	1/2	51486	15907(600)	
	3/2	60608	28958(900)	
$5d^{-1}6s6p$	5/2	79705	$-35788(400)$	
$5d^{-1}6s6p$	7/2	84212	$-34233(400)$	
	5/2	84836	$-33158(300)$	
	3/2	86178	$-32654(700)$	

[a]Reference [21].
[b]Reference [22].

Therefore we extract an updated limit on time variation of α of $\dot{\alpha}/\alpha = (-1.8 \pm 2.8) \times 10^{-17}$/yr.

VI. CONCLUSION

We have presented a particle-hole CI+MBPT theory that provides more flexibility than previous versions. In particular, it should be able to accurately calculate systems that are better treated with holes, access particle-hole excitations, and give us the choice to treat correlations with filled core shells either perturbatively using MBPT or nonperturbatively using CI. We have applied the method to low-lying transition energies in Hg$^+$, including the optical clock transition, which to lowest order is a particle-hole excitation.

The current limitation of our method is in the energy denominators of Eq. (9). In keeping with our previous CI+MBPT methods, we have employed Brillouin-Wigner perturbation theory (see [2] for details), but this cannot be an accurate treatment for all levels. Methods to treat the energy denominators to higher order have been developed, such as including $\partial\Sigma/\partial E$ [1] or simple addition of an offset in the denominator [23,28], and these may improve our accuracy in the future. The particle-hole CI formalism can also be combined with other methods used to calculate core-valence correlations, such as the all-order correlation potential [29,30] or singles-doubles coupled-cluster [31] methods.

[1] V. A. Dzuba, V. V. Flambaum, and M. G. Kozlov, Phys. Rev. A **54**, 3948 (1996).

[2] J. C. Berengut, V. V. Flambaum, and M. G. Kozlov, Phys. Rev. A **73**, 012504 (2006).

[3] J. C. Berengut, V. V. Flambaum, A. Ong, J. K. Webb, J. D. Barrow, M. A. Barstow, S. P. Preval, and J. B. Holberg, Phys. Rev. Lett. **111**, 010801 (2013).

[4] A. Ong, J. C. Berengut, and V. V. Flambaum, Phys. Rev. A **88**, 052517 (2013).

[5] I. M. Savukov, Phys. Rev. A **91**, 022514 (2015).

[6] J. C. Berengut, V. V. Flambaum, and E. M. Kava, Phys. Rev. A **84**, 042510 (2011).

[7] S. G. Porsev, K. V. Koshelev, I. I. Tupitsyn, M. G. Kozlov, D. Reimers, and S. A. Levshakov, Phys. Rev. A **76**, 052507 (2007).

[8] V. A. Dzuba, Phys. Rev. A **71**, 032512 (2005).

[9] A. Windberger, J. R. Crespo López-Urrutia, H. Bekker, N. S. Oreshkina, J. C. Berengut, V. Bock, A. Borschevsky, V. A. Dzuba, E. Eliav, Z. Harman, U. Kaldor, S. Kaul, U. I. Safronova, V. V. Flambaum, C. H. Keitel, P. O. Schmidt, J. Ullrich, and O. O. Versolato, Phys. Rev. Lett. **114**, 150801 (2015).

[10] J. C. Berengut, V. A. Dzuba, V. V. Flambaum, and A. Ong, Phys. Rev. Lett. **106**, 210802 (2011).

[11] M. T. Murphy and J. C. Berengut, Mon. Not. R. Astron. Soc. **438**, 388 (2014).

[12] V. A. Dzuba, V. V. Flambaum, M. G. Kozlov, and M. Marchenko, Phys. Rev. A **66**, 022501 (2002).

[13] I. M. Savukov, W. R. Johnson, and H. G. Berry, Phys. Rev. A **66**, 052501 (2002).

[14] I. M. Savukov, J. Phys. B **36**, 4789 (2003).

[15] I. M. Savukov, J. Phys. B **36**, 2001 (2003).

[16] I. M. Savukov, Phys. Rev. A **85**, 052512 (2012).

[17] D. J. Berkeland, J. D. Miller, J. C. Bergquist, W. M. Itano, and D. J. Wineland, Phys. Rev. Lett. **80**, 2089 (1998).

[18] S. A. Diddams, Th. Udem, J. C. Bergquist, E. A. Curtis, R. E. Drullinger, L. Hollberg, W. M. Itano, W. D. Lee, C. W. Oates, K. R. Vogel, and D. J. Wineland, Science **293**, 825 (2001).

[19] M. Simmons, U. I. Safronova, and M. S. Safronova, Phys. Rev. A **84**, 052510 (2011).

[20] T. Rosenband, D. B. Hume, P. O. Schmidt, C. W. Chou, A. Brusch, L. Lorini, W. H. Oskay, R. E. Drullinger, T. M. Fortier, J. E. Stalnaker, S. A. Diddams, W. C. Swann, N. R. Newbury, W. M. Itano, D. J. Wineland, and J. C. Bergquist, Science **319**, 1808 (2008).

[21] V. A. Dzuba, V. V. Flambaum, and J. K. Webb, Phys. Rev. A **59**, 230 (1999).

[22] V. A. Dzuba and V. V. Flambaum, Phys. Rev. A **77**, 012515 (2008).

[23] J. C. Berengut, V. V. Flambaum, and M. G. Kozlov, J. Phys. B **41**, 235702 (2008).

[24] W. R. Johnson, S. A. Blundell, and J. Sapirstein, Phys. Rev. A **37**, 307 (1988).

[25] P. O. Schmidt, T. Rosenband, C. Langer, W. M. Itano, J. C. Bergquist, and D. J. Wineland, Science **309**, 749 (2005).

[26] T. Rosenband, P. O. Schmidt, D. B. Hume, W. M. Itano, T. M. Fortier, J. E. Stalnaker, K. Kim, S. A. Diddams, J. C. J. Koelemeij, J. C. Bergquist, and D. J. Wineland, Phys. Rev. Lett. **98**, 220801 (2007).

[27] E. J. Angstmann, V. A. Dzuba, and V. V. Flambaum, Phys. Rev. A **70**, 014102 (2004).

[28] M. G. Kozlov and S. G. Porsev, Opt. Spectrosc. **87**, 352 (1999).

[29] V. A. Dzuba, V. V. Flambaum, and O. P. Sushkov, Phys. Lett. A **140**, 493 (1989).

[30] V. A. Dzuba, Phys. Rev. A **78**, 042502 (2008).

[31] M. S. Safronova, M. G. Kozlov, W. R. Johnson, and D. Jiang, Phys. Rev. A **80**, 012516 (2009).